

We are IntechOpen, the world's leading publisher of Open Access books Built by scientists, for scientists

6,900

Open access books available

186,000

International authors and editors

200M

Downloads

Our authors are among the

154

Countries delivered to

TOP 1%

most cited scientists

12.2%

Contributors from top 500 universities



WEB OF SCIENCE™

Selection of our books indexed in the Book Citation Index
in Web of Science™ Core Collection (BKCI)

Interested in publishing with us?
Contact book.department@intechopen.com

Numbers displayed above are based on latest data collected.
For more information visit www.intechopen.com



Nanostructured Titanium Dioxide for Functional Coatings

Indriana Kartini, Inna Yusnita Khairani, Chotimah, Kuwat Triyana and Sri Wahyuni

Additional information is available at the end of the chapter

<http://dx.doi.org/10.5772/intechopen.74555>

Abstract

Synthesis routes to nanostructured titanium dioxides (spherical nanoparticles, nanotubes, mesostructure) have been studied. Their potential applications in various fields based on coating technology have been explored, i.e., dye-sensitized solar cells (using ruthenium sensitizer and some results of natural dyes), photocatalysts for self-cleaning films (TiO_2 on textiles), antibacterial coating for multifunctional textiles ($\text{TiO}_2\text{-SiO}_2$ on cotton), and recent result on antifouling coating on wood. The synthesis/preparation procedures were developed to obtain green protocols based on combined techniques of hydro- or solvo-thermal (templated, seeded, deposition), sol-gel (templated, room temperature, dip coating), and solvent-casting techniques. Discussion on the properties and synthesis mechanism is presented. It will be shown that sonication has important role to shorten the preparation of nanotube titania and has been proposed as one green synthesis route. The changing of morphology of titanium dioxide has presented unexpected results to the shifting of photoactivity into visible irradiation.

Keywords: nanostructure, TiO_2 , solar cells, photocatalyst, functional textile, antibacterial

1. Introduction

Titanium dioxide (TiO_2), so-called titania, has shown excellent properties for functional coating materials. As a semiconductor, it functions as photoactive materials. Designing the morphology down to the scale of nanometer, which is called nanostructured, results in some new properties to be envisaged. Synthesis routes are designed to achieve the desired properties

for certain applications. A high-surface-area titania is beneficial as photoanode in photoelectrochemical solar cells to obtain efficient light harvesting due to the characteristics of dye-monolayer adsorption. However, high surface area is not enough for efficient photoanodes. The titania must also have high crystallinity of the photoactive phase, which is mostly anatase crystalline phase. The presence of microporosity is not favorable for the dye adsorption, hindering efficient dye adsorption. Previous studies have shown that there is a compromise between high surface areas with porosity and crystallinity of the anatase phase [1–3]. For multifunctional textiles, amorphous titania is favored due to strong adherence to the surface of the cellulose-based fabrics [4] compared to the crystalline phase of titania. Interestingly, 1D-nanostructured titania, such as nanorods or nanotubes, has shown notable photocatalytic activity under the visible light irradiation.

Here, synthesis route to obtain high-surface-area titania with full domain of anatase phase will be presented and discussed. Some results for the application of the resulted mesostructured titania for dye-sensitized solar cells (DSSC) will be included. Secondly, applications to functional coating for textile and wood are also deliberated by considering photocatalytic and hydrophilic/hydrophobic mechanism. Combining nanostructured titania and silica resulted in excellent antibacterial coatings. Recent results of nanorod titania and silica as antifouling coating on wood are presented.

2. Synthesis routes to nanostructured titanium dioxides (mesostructure spherical nanoparticles, nanotubes)

Firstly, mesostructured titania as photoanodes for photoelectrochemical solar cells that are famously called dye-sensitized solar cells (DSSC) is discussed. Hydrothermal-seeded protocol is offered as a recommended synthesis route to achieve the targeted photoactivity. Secondly, one-dimensional nanostructured titania is proposed for the photoanodes. Nanotube titania was synthesized through templated-hydrothermal method and has shown improved photoactivity than that of nanoparticles. Sonication is proposed to shorten the synthesis time to prepare nanotube titania.

2.1. Hydrothermal-seeded synthesis of mesostructured titania

Synthesis of nanostructured titanium dioxides has been greatly explored and discussed. The hydrothermal-seeded synthesis route was inspired by a similar approach in preparing mesoporous aluminosilicates containing zeolite framework [5–8]. The auto-assembly zeolite seed concept was applied by creating anatase seeds to the synthesis of mesoporous titania. Basically, there are three main steps in the synthesis route, namely, anatase seed preparation, hydrothermal self-assembly, and template removal. Anatase phase was chosen as the nanocrystal seed due to its highest photocatalytic activity among other crystalline phases of titania. Instead, some studies showed that it is easy to obtain such phase at low temperature and short-time synthesis [9, 10]. Anatase is also well known as a kinetically favored crystalline phase of titania for most synthesis routes. In this study, the anatase seeds prepared via neutral

and acidic route (**Figure 1**) are discussed. Hydrothermal interaction between block-copolymer surfactant and the anatase seeds is illustrated. Results on the adsorption of Ru-“black dye” onto selected powders are included.

The preparation of anatase seed is aimed at obtaining nanocrystals with less than 5 nm size, as the thickest wall obtained for mesoporous titania so far does not exceed 5 nm [11]. Hydrothermal technique was proposed to be the technique of choice to prepare the anatase seeds, due to its simplicity and its good reproducibility [9]. The resultant materials were then examined either by XRD or TEM for the presence of the anatase nanocrystals.

Two main routes of the seed preparation, as displayed in **Figure 1**, were proposed. It comprises the hydrothermal hydrolysis and condensation of titanium precursor at a neutral and an acidic condition. A mixture of ethanol in water was used as the hydrolysis media. Ethanol was introduced as a cosolvent to slightly slow down the hydrolysis and condensation rates. It was also chosen to obtain higher oxide content from the hydrolytic condensation of titanium (IV) tetraisopropoxide compared to the process using its parent alcohol [12]. Then, in the second route, acid is introduced to further retard the condensation [13, 14] and obtain clear solution seeds. **Figures 2** and **3** show the dark- and bright-field TEM images of the resulted anatase seeds resulted from neutral and acidic solution, respectively.

The seed suspensions were obtained after 4 h hydrothermal treatment at 80°C. The bright- and dark-field TEM images of this seed as well as its selected area electron diffraction (SAED) pattern are presented in **Figure 2**. Diffuse ring SAED pattern indicates the formation of a very small polycrystalline material, which has been indexed as the anatase crystal phase of titania [1]. The presence of bright spots all over the sample region shows the uniform distribution of these crystal phases, while the magnified image in the dark-field TEM image presents the observed lattice strain from [101] anatase phase. Based on the TEM image, the crystal size is around 5 nm as designed. However, the seed solution was a milky solution. Anatase seeds obtained from neutral hydrothermal route can be recovered as a very light powder.

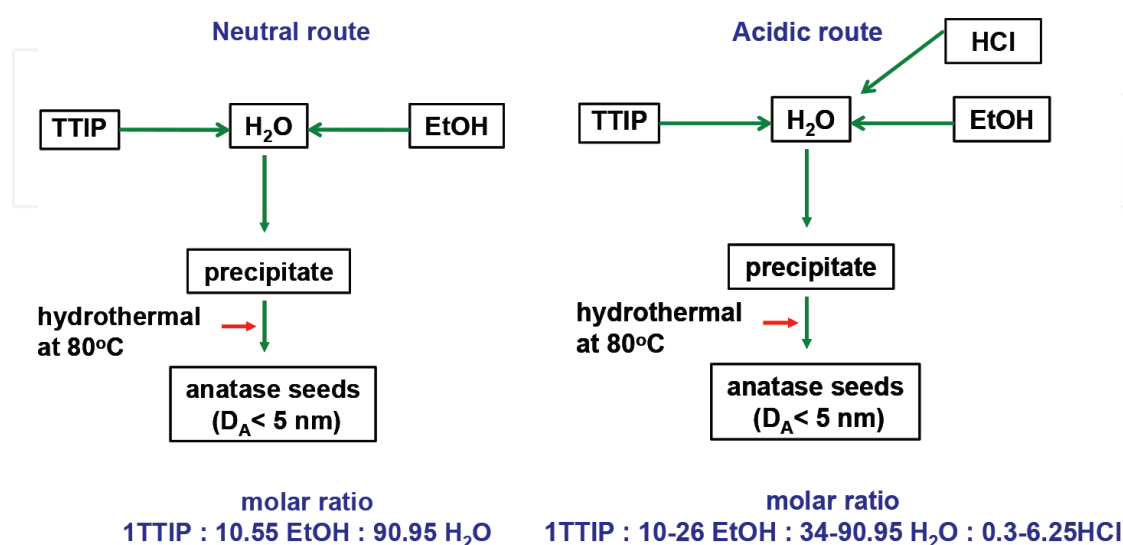


Figure 1. Flow diagram of the approach used in anatase seed preparation via hydrothermal technique.

The acidic route was proposed in order to obtain an ideal clear seed solution containing the desired crystalline phase as applied in zeolitic-aluminosilicate synthesis. Previous study has proven the importance of introducing acid to stabilize colloidal particles resulted during hydrolysis-condensation reaction and obtaining transparent solution [12, 15]. Variation on the acid concentration can be altered to obtain fewer amounts of HCl for such purpose. HCl is also known to accelerate the anatase nucleation [10], which will be beneficial for hydrothermal process at low temperature. Since the seed is a clear solution, TEM was used to examine the crystal size and phase by using dark-field/bright-field images at the same area and selected area electron diffraction, respectively.

Figure 3 displays the bright- and dark-field TEM images of anatase seed resulted from the acidic route with molar ratio precursor composition of 1TTIP:26.10EtOH:34.06H₂O:1.25HC

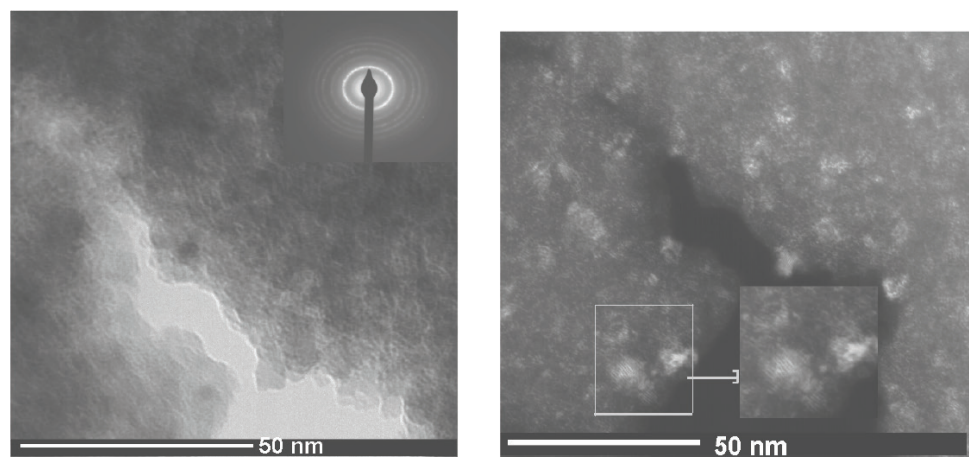


Figure 2. Bright-field TEM image with the respective SAED pattern (left) and the dark-field (right) [1] TEM image of anatase seed solution prepared hydrothermally at 80°C for 4 h and neutral condition.

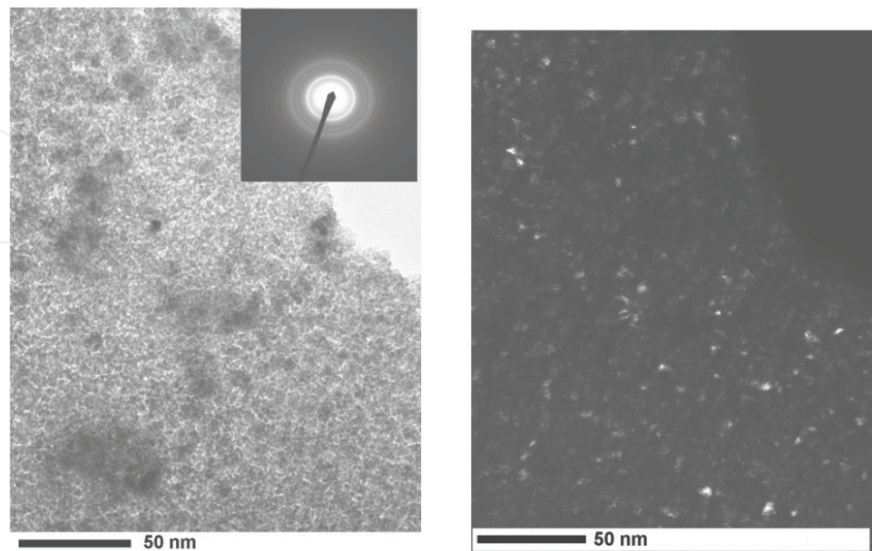


Figure 3. Bright-field TEM image with the respective SAED pattern (left) and the dark-field (right) TEM image of anatase seed solution prepared hydrothermally in acidic solution at 80°C for 4 h.

1. The bright spots observed in the dark-field images confirm the formation of nanocrystals. From **Figures 2** and **3**, it can be seen that the presence of acidic strength resulted in smaller crystalline phase, which are averaged at 2.05 nm. As a result of such small crystallites, the SAED of the seed from acidic route (indexed as an anatase phase) is more diffuse compared to that of the anatase seed obtained from neutral route. The seed solution is hazy. Those two anatase seeds were then proceeded into step 2 hydrothermal synthesis which is mesoporous titania synthesis.

Table 1 lists the textural parameters of the resulted titania powders synthesized at various condition of hydrothermal temperature and time, while **Figure 4** displays the N₂ adsorption–desorption isotherms as well as the corresponding pore size distribution (BJH model desorption branch) of calcined mesoporous titania obtained from hydrothermal interaction between neutral route-derived anatase seed and neutral aqueous surfactant solution. The second step of hydrothermal synthesis involved block copolymer, P123 as the pore template [1, 2]. **Figure 5** shows the N₂ adsorption–desorption isotherms as well as the corresponding pore size distribution (BJH model desorption branch) of calcined mesoporous titania obtained from hydrothermal interaction between neutral route-derived anatase seed and neutral aqueous surfactant solution.

From **Table 1** and **Figure 4**, it can be seen that the time alternation at given temperature does not change significantly the isotherm type, as well as the surface area and pore diameter. Type IV isotherm of typical mesoporous materials with well-defined hysteresis loops was obtained. However, the pore size distribution is much broadened at shorter (5 h) or longer (48 h) hydrothermal treatment, more likely due to insufficient interaction or disrupted interaction, respectively, between anatase seed and block copolymer micelles. On the other hand, effect of hydrothermal temperature is much pronounced on surface area, pore size, and pore volume as demonstrated in **Table 1** and **Figure 5**. Type IV isotherms with hysteresis loop corresponding to the ordered mesopore filling are evidenced. The relative pressure of pore filling increases with hydrothermal temperature. Thus, an increase of pore size and a decrease in the surface area with the hydrothermal temperature are observed. Pore size broadening is

Sample ¹	S _{BET} (m ² /g, STP)	V _p (cm ³ g ⁻¹)	BJH pore diameter (nm)
Hydrothermal 100°C, 5 h	101.00	0.26	7.86
Hydrothermal 100°C, 10 h	100.90	0.24	7.83
Hydrothermal 100°C, 20 h	106.00	0.23	7.72
Hydrothermal 100°C, 48 h	110.40	0.27	7.89
Hydrothermal 80 °C, 20 h	152.30	0.29	6.19
Hydrothermal 100°C, 20 h	106.00	0.23	7.72
Hydrothermal 150°C, 20 h	98.70	0.24	7.90

¹TTIP:P123:EtOH:H₂O = 1:0.034:10.55:431.6 (molar ratio precursor composition).

Table 1. Textural parameters of mesoporous titania resulted from neutral route anatase seed and neutral aqueous surfactant.

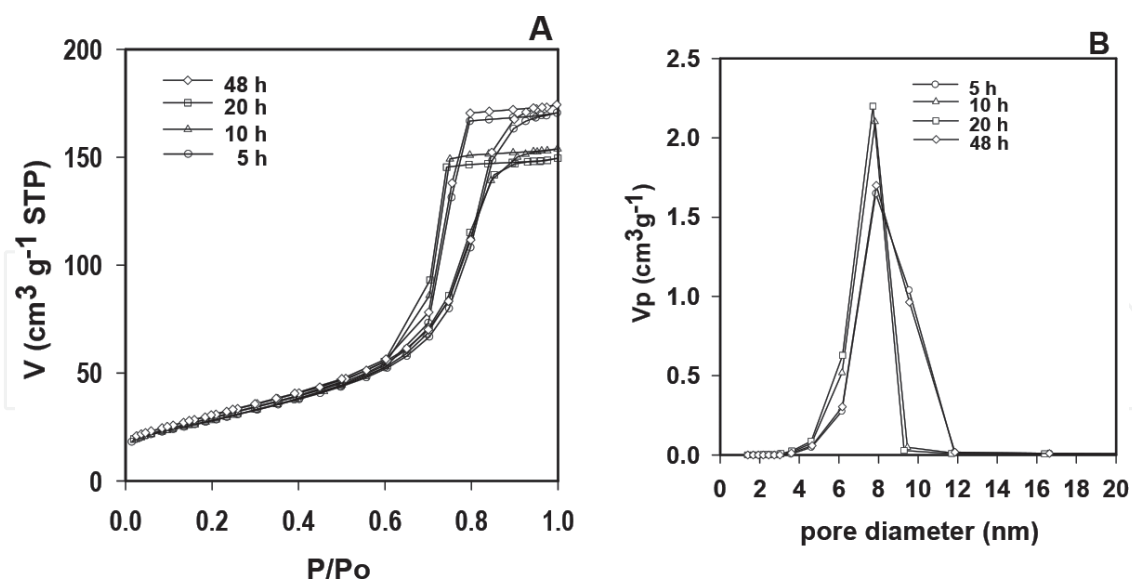


Figure 4. N_2 adsorption–desorption isotherms (A) and pore size distribution (B) of mesoporous titania synthesized from neutral anatase seed and neutral surfactant solution at various hydrothermal times at 100°C after calcination at 400°C.

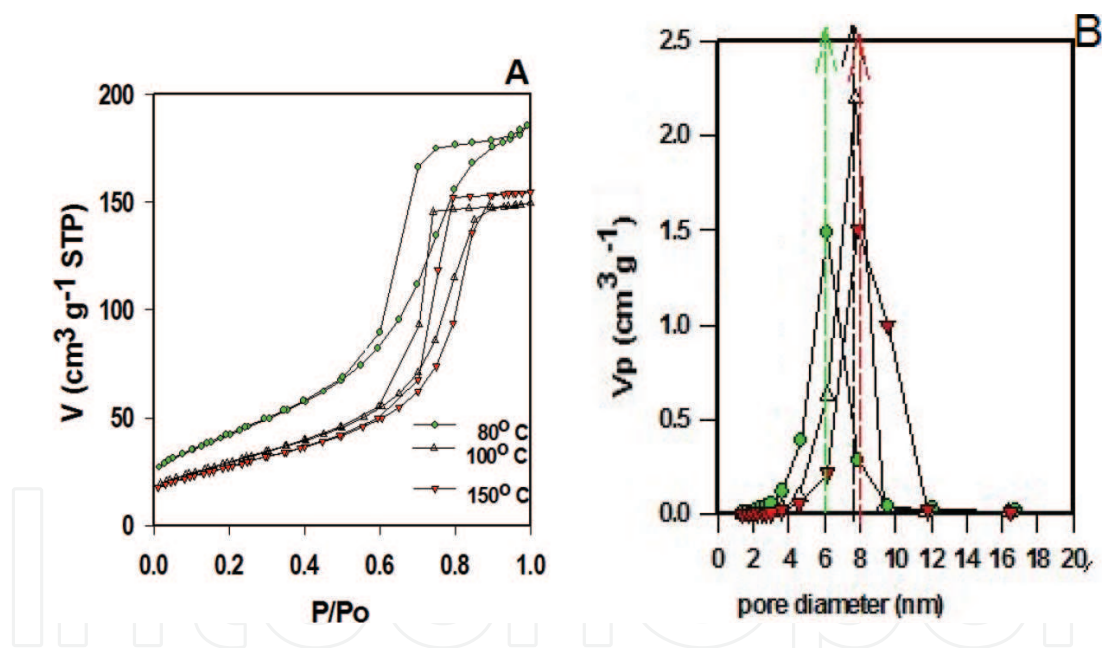


Figure 5. N_2 adsorption–desorption isotherms and pore size distribution of mesoporous titania synthesized from neutral anatase seed and neutral surfactant solution at various hydrothermal temperatures for 20 h after calcination at 400°C.

prominent at 150°C hydrothermal treatment, which is likely due to phase separation of the block copolymer template at temperature higher than its *cloud point* (85°C for P123 in aqueous neutral solution) [16, 17]. At higher temperature than its *cloud point*, micelle-micelle interaction is getting more prominent as water becomes less effective solvent for the polyethylene oxide (PEO) chains, resulting in strong micelle-micelle aggregation. Therefore the micelle aggregate size is getting bigger, directing the formation of larger pores. The interaction is illustrated in **Figure 6**.

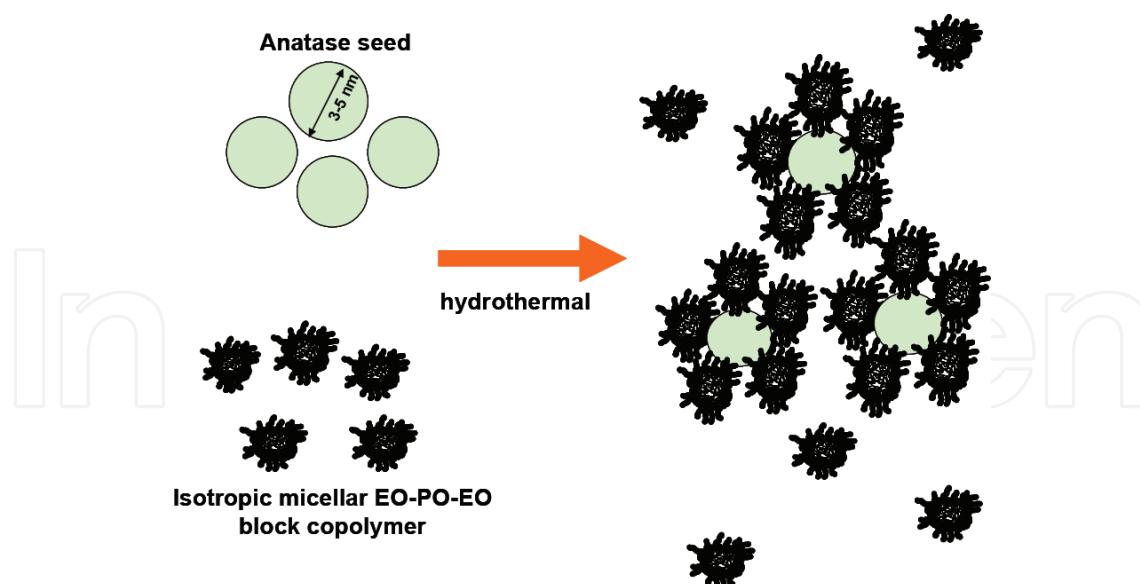


Figure 6. Illustration of micelle-stabilized anatase seed aggregation mechanism during hydrothermal treatment.

At 80°C hydrothermal treatment, the low-angle XRD peak (data not shown) appears as a shoulder around $1.5^\circ 2\theta$, indicating less order mesopore structuration as implied by the presence of broad hysteresis loop in its N_2 adsorption–desorption isotherm as well. Higher hydrothermal temperature results in broad low-angle XRD peak, indicating possible mesopore distribution broadening. This fact is also evidenced by its pore size distribution obtained using N_2 adsorption–desorption analysis.

On the other hand, anatase seed undergoes transformation into rutile crystalline phase at 150°C (data not shown). The high temperature results in rapid crystallization owing to a favored dissolution precipitation mechanism [10], which allows the fast transformation from anatase to rutile crystalline phase. It has been shown that anatase seed treated hydrothermally with aqueous block copolymer solution at 100°C for 20 h exhibits highest porosity with ordered mesopores and full anatase crystalline domain [1]. The TEM images of the resulted powder can be found elsewhere [1].

From the TEM images, it is clear that block copolymer functions to aid pore organization without showing template mechanism as usually observed in micelle-templated silica or metal oxide using the same nonionic surfactant [11, 16–19]. The possible mechanism is assumed to be an aggregation mechanism over block copolymer-steric stabilized-anatase seed particles. $EO_{20}PO_{70}EO_{20}$ is known to form spherical micelles, with the dense cores consisting of dehydrated PO blocks and hydrated EO blocks at the micellar surface (coronas), at critical micellar concentration (cmc) of 0.03 wt% at 25°C in water [20, 21].

The micelles are attached to the anatase seed via their protruded-EO chains in such a way covering the anatase surface, creating steric stabilization to the anatase seeds. Such interaction is likely driven by a surface charge potential between the micelles and anatase seeds. Control over pore formation and crystalline growth is attained by a corona of block copolymer micelles formed around anatase seed particles as illustrated in **Figure 6**. The subsequent

removal of the block copolymer leads to interstitial pore arrangements resulting in the formation of uniform and well-controlled mesopores.

Table 2 tabulates the textural porosity of the resultant powders derived from hydrothermal interaction between acidic route anatase seeds with neutral aqueous surfactant. Subjecting acidic route anatase seed for longer hydrothermal treatment with acidic aqueous surfactant results in different effects to the porosity of the resultant calcined powders. Larger pores are created, while they present type IV isotherm with type H2 hysteresis loops (**Figure 7**). As predicted, prolonged hydrothermal treatment induces the formation of wide pore size distribution (**Figure 7** and **Table 2**). The crystalline phase is assigned as the anatase titania. Our study for higher acidity of the anatase seed resulted in a mixture of crystalline phase of anatase and rutile titania (data not shown).

Figure 8 shows the UV–Visible spectra of the Ru-“black dye” solution before and after overnight adsorption using the respective mesoporous titania powder synthesized hydrothermally from anatase seeds, as the adsorbents. Porosity characteristics of the samples are summarized in **Table 3**. It is clear that the powders resulted from anatase seed hydrothermal synthesis demonstrates significant adsorption of Ru-“black dye.” Correlating the adsorption

Sample ¹	S _{BET} (m ² /g,STP)	V _p (cm ³ g ⁻¹)	Pore diameter (nm)
Hydrothermal 100°C, 40 h	156.70	0.46	9.70
Hydrothermal 100°C, 65 h	152.00	0.44	9.72
Hydrothermal 100°C, 90 h	127.30	0.47	12.52
Hydrothermal 100°C, 190 h	128.80	0.44	9.71

¹TTIP:0.034P123:26EtOH:2.8HCl:170H₂O; [H⁺] = AS-1 < AS-2~AS<AS-3.

Table 2. Textural parameters of mesoporous titania resulted from acidic route anatase seed and neutral aqueous surfactant.

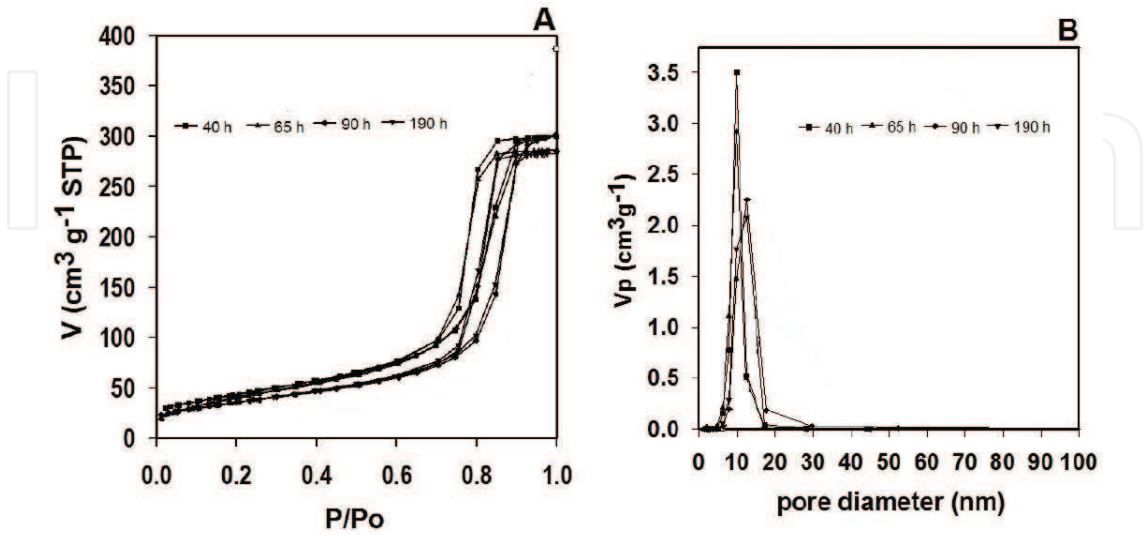


Figure 7. (A) N₂ adsorption–desorption isotherms and (B) pore size distribution of mesoporous titania synthesized at various hydrothermal times from acidic route anatase seeds’ neutral aqueous surfactant.

capability with textural properties of the powders, large pore samples perform higher ability to adsorb the dye molecules. Therefore, it is confirmed that the presence of large pore with appreciable porosity is favorable for dye adsorption to sensitize titania photoanode in photoelectrochemical solar cells. The optimum peaks of the dye solution after adsorption have shifted to higher wavelengths due to possible dye oxidation during the measurement. The discussion on the DSSC performance will be on Section 3. Based on the textural properties and the resulted crystalline phase of anatase titania, mesostructured titania from hydrothermal-seeded synthesis are suitable for photoanodes of DSSC.

2.2. Hydrothermal synthesis of 1D nanostructured titania

The needs to get high surface area for DSSC and also photocatalysis encourage the search to utilize 1D-nanostructured titania, such as nanotube, nanorods, and/or nanofibers. Interest to the

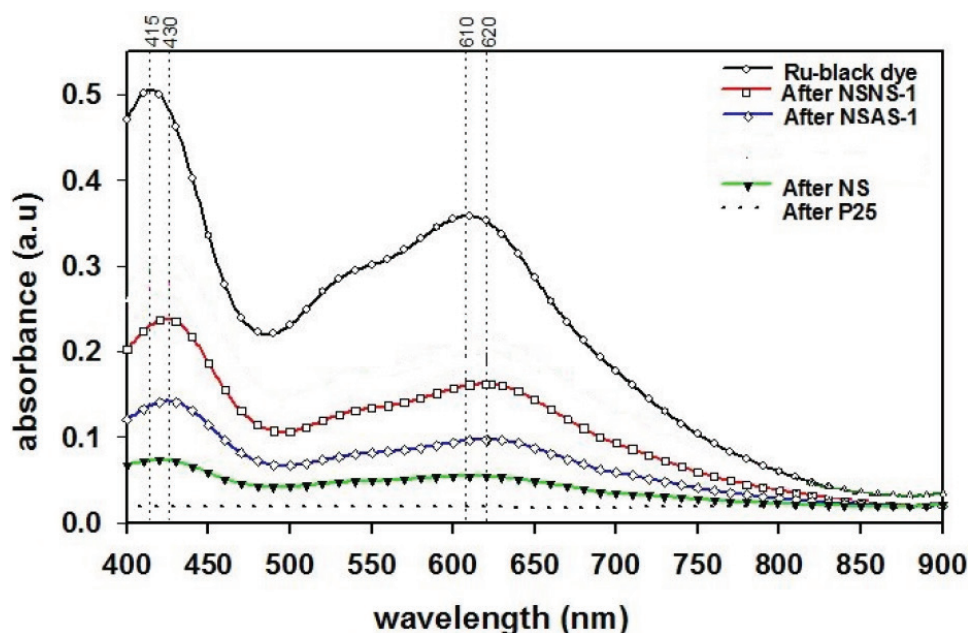


Figure 8. Absorbance of ruthenium-“black dye” after various hydrothermal-derived mesoporous titania powder adsorption. A commercial titania Degussa P25 was used as comparison.

Sample	Pore volume (cc/g)	Dp (nm) BJH _d	S _{BET} (m ² /g)	Isotherm/hysteresis loop type	Dye adsorbed (%)
NSNS-1	0.48	9.66, 60.60	146.50	II-IV/H1-H2	61.20
NSAS-1	0.54	12.61	118.70	IV/H2	81.28
P25 (Degussa)	0.10	74.2	55.74	II	>99.00

NS = neutral anatase seed, NSNS = neutral anatase seed + neutral surfactant, NSAS = neutral anatase seed + acidic surfactant, NSNS-1 = 1.25 g P123/40 mL H₂O, NSAS-1 = 3.2 g P123/(40 mL H₂O + 4 mL HCl).

Table 3. Ru-“black dye” adsorption onto selected calcined mesostructured titania along with their corresponding textural properties.

structure is mostly due to the surface area. Nanotube with open-ended tube structure may have surface area of $\sim 400 \text{ m}^2/\text{g}$ [22]. Nanorods or nanofibers may only have $50 \text{ m}^2/\text{g}$ [23]. Therefore, the synthesis then is focused at obtaining titania nanotubes. Titania nanotubes can be achieved via alkaline hydrothermal method which is the most promising method, because of its simplicity and high reproducibility. Excess concentrated alkaline of 10 M NaOH is commonly used as the hydrothermal medium at low temperature of $110\text{--}150^\circ\text{C}$ for 24 h to obtain sodium titanate nanotube. Washing with dilute acid and heating may lead the sodium titanate to transform into anatase crystalline phase via the formation of hydrogen titanate and $\text{TiO}_2(\text{B})$ [23].

Using excessive amount of highly concentrated and corrosive base such as NaOH is not environmentally benign. This encourages several researches to alternate and study the effect of alkaline alteration. A vapor pressure by using $\text{NH}_3(\text{aq})$ during the hydrothermal is one of the quests [24]. However, bundles of nanotubes could only be formed by the presence of KOH. It was found that only KOH and NaOH are the contributing alkaline medium for nanotube formation. The spherical titania will not transform into nanotube by the presence of LiOH_2 or NH_3 . Successful route without NaOH(aq) in the solvent was proposed by Liu et al. [25] involving titania foil covered with NaOH as the titania source. They proposed scrolling mechanism induced by NH_3 vapor pressure to transform titania nanosheets into nanotubes. NaOH was needed to make the titania nanosheets. Steps for the transformation of TiO_2 to nanotubular titanate can be summarized as follows: first, the dissolution of the TiO_2 sources, at the same time, to the growth of layered nanosheets of sodium trititanates. Secondly, nanosheets are curving and then wrapping into nanotubes [23].

The as synthesized products from hydrothermal method were titania with titanate crystalline phases, which were sodium trititanate or hydrogen trititanate, as depicted in **Figure 9** (right). These phases are not favored for the DSSC, due to its low photocatalytic activity [26]. Later, efforts to induce the anatase phase formation by acid washing and calcination are introduced. Care must be taken for using the acid, since too acidic medium exceeding the pH of 3 may ruin the tube structure [27, 28]. By applying calcination, the anatase crystalline phase starts to form at 200°C and complete at 500°C [29]. High temperature may lead to breaking up of nanotube structure [30]. Therefore, the optimum conditions for acid washing and calcination temperature are needed to obtain anatase TiO_2 with nanotube morphology.

In this research, the way to alter or reduce the amount of NaOH in the alkaline hydrothermal method was sought, by using NH_3 as the solvent combined by NaOH, at high concentration level for both solutions. Then, posttreatments, in particular the acid washing and calcination temperature, were introduced. The synthesis protocol for these nanotubes can be found elsewhere [31]. **Figure 9** shows the TEM images of the resulted titania synthesized using NaOH with (Na-Ti-DW) and without acid washing (Na-Ti-H), as well as using a mixed solution of NH_3 and NaOH (1:3 molar ratio) with acid washing.

The TEM images (**Figure 9** left) show nanotube structure without the presence of other structures, such as nanorods or nanoparticles. Images of TEM show dispersed TiO_2 nanotubes with diameter around 3–5 nm and outer diameter of 8–12 nm. Nanotube lengths are ranging from 80 to 400 nm. The selected area electron diffraction (SAED) was taken to define the crystallinity of a certain area in the sample (**Figure 9** right). Sample Na-Ti-DW exhibits diffuse ring

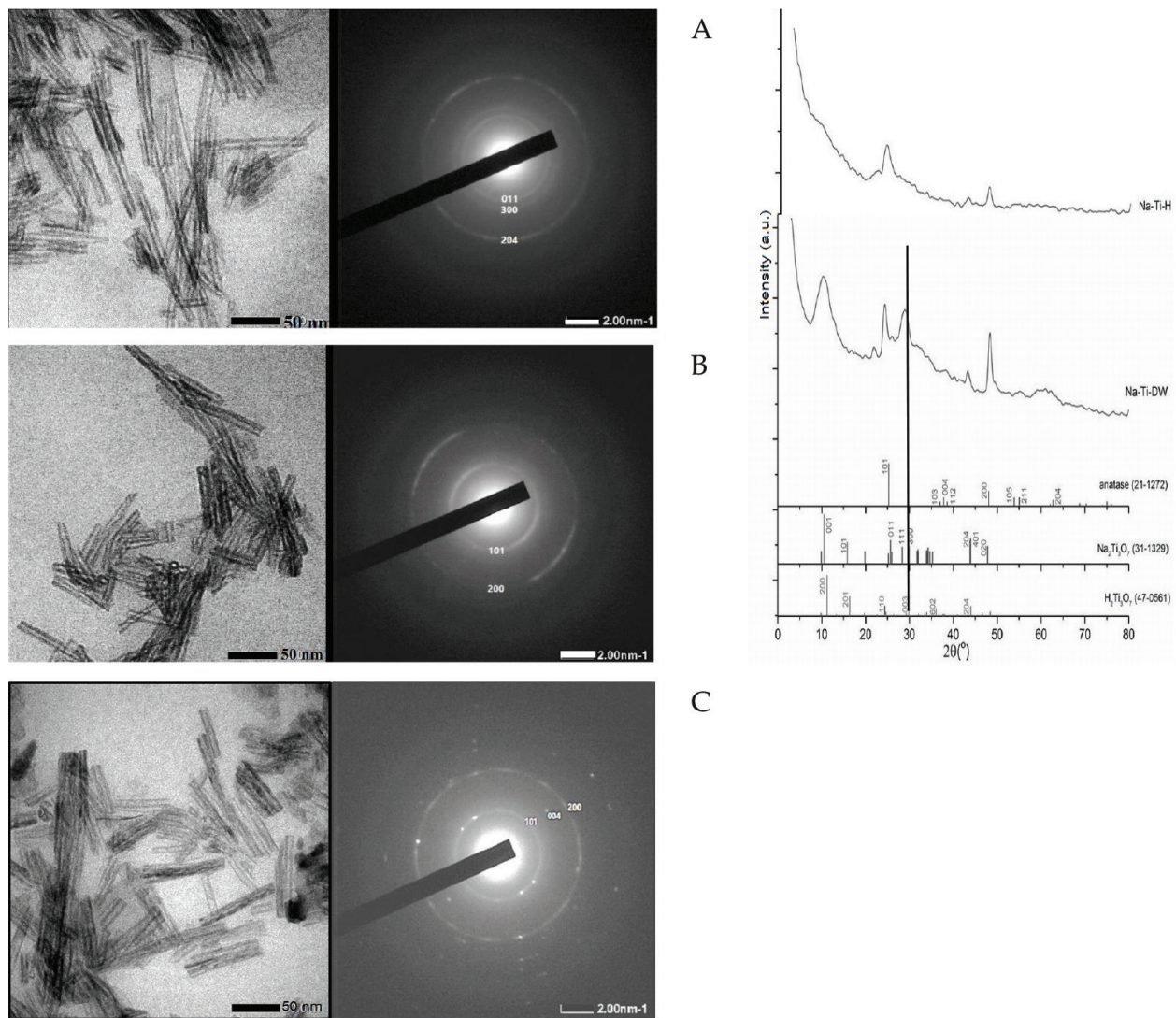


Figure 9. Bright-field TEM images of sample (left), the corresponding SAED pattern (middle) of (A) Na-Ti-DW, (B) Na-Ti-H, and (C) 3:1 NaNH₃-Ti-H and XRD patterns (right) of Na-Ti-DW and Na-Ti-H.

pattern and low-intensity diffraction, which identifies the contributions of amorphous material instead of polycrystalline materials. It has diffraction at crystal plane [011], [300], and [204] that belong to sodium trititanate phase. To ensure the materials crystallinity, XRD pattern was also taken to obtain the contributing crystalline phase of the sample. The XRD results show that the crystalline phase of sample Na-Ti-DW has strong peaks at $2\theta \approx 10.5^\circ$, 24° , 28° , 43° , and 48° similar to the XRD pattern by Sikhvivilu et al. [24], with distinct peak at $2\theta \approx 10^\circ$ and low-intensity peaks at $2\theta \approx 24^\circ$, 28° , and 48° . It is indicated that the as synthesized product has the similar crystalline phase, which is predominantly titanate phase. It is confirmed as sodium trititanate (PDF 31–1329). The sample Na-Ti-DW also bears amorphous, signified from the bland feature at around $2\theta \approx 30^\circ$ and 60° , and anatase (PDF 21–1272) phase, identified from reflections at $\sim 24^\circ$ (d_{101}) and 60° (d_{200}). For Na-Ti-H, the XRD pattern shows the diminishing peaks of sodium trititanate phase. It is found that the synthesis of nanotubes with water washing treatment (Na-Ti-DW) exhibits titanate nanotube, while with dilute acid (Na-Ti-H),

it produces anatase crystalline phase. Diffraction at $2\theta \approx 24^\circ$ is probably due to the shifts from peak at 25° of anatase (101) and titanate (011). Peak shifts are preferred due to the formation of nanotubes, which put strains on the bonding in sample. The corresponding Raman spectra published elsewhere [31] support the formation of anatase phase after acid washing.

The morphological structure for sample 3:1 $\text{NaNH}_3\text{-Ti-H}$ (**Figure 9C**) with 3:1 base ratio ($\text{NaOH}:\text{NH}_3$) was found to be similar with Na-Ti-H , as mostly all of the morphology of titania were open-ended nanotubes. The nanotubes are highly distributed (separated from each other), showing that the bundles of titania did not form. Yet a few nanosheets are visible in the image, confirming that the morphological changes did not perfectly occur. High amount of NH_3 leads to the transformation from nanotubes into nanosheets and later to spherical structures [31]. Thus, nanotube preparation can be sought at NH_3 ratio to NaOH of 1:3. Alteration to only using NH_3 as the alkaline results in the formation of spherical nanoparticle titania with anatase crystalline phase [31].

Short-time synthesis of titania nanotube was proposed by applying mechanical or sonication-assisted stirring prior hydrothermal. The effect of various stirring times and hydrothermal treatments on the crystalline phases and morphology of the resulted titania has been studied [32]. It has been shown that the nanotube titania can be obtained after 5 h hydrothermal treatment at 150°C . The XRD patterns of the resulted powders showed the existence of a mixture of anatase and titanate crystalline phases with increased intensity of [200] as the stirring time increasing. At the longest stirring time, the existence of TiO_2 (B) was observed. Raman spectra have also confirmed the existence of both anatase and titanate crystalline phases. The high textural coefficient for [200] (TC_{200}) has indicated oriented growth of one-dimensional anatase along [200]. All powders resulted at various stirring time were nanotubes, as confirmed by transmission electron microscope (TEM).

The next section will discuss the application of titanium dioxide for photoelectrochemical solar cells (DSSC) and multifunctional coatings for textiles and woods.

3. Titania as the photoanode for dye-sensitized solar cells

The dye-sensitized solar cell consists of three main components, namely, a working electrode, a counter electrode, and an electrolyte. The current most efficient cells of 10.4% [33] used a nanostructured titanium dioxide film on a transparent conducting glass (TCO) as a working electrode, a platinized conducting glass as the counter electrode and I_3 pairs as the electrolyte solution. In this section, performance of the mesoporous titania electrodes as photoanodes in DSSCs is presented. Some results using natural dyes as the photosensitizers will also be discussed.

Since the anatase crystalline phase seems to be preferred for this DSSC, attempts to incorporate the neutral route hydrothermal powder into a DSSC were carried out. A one-coat slip-cast electrode was assembled with sputtered and thermally platinized counter electrodes. **Figure 10** shows the I-V curves of these DSSCs using ruthenium "N3" as the sensitizer by using different

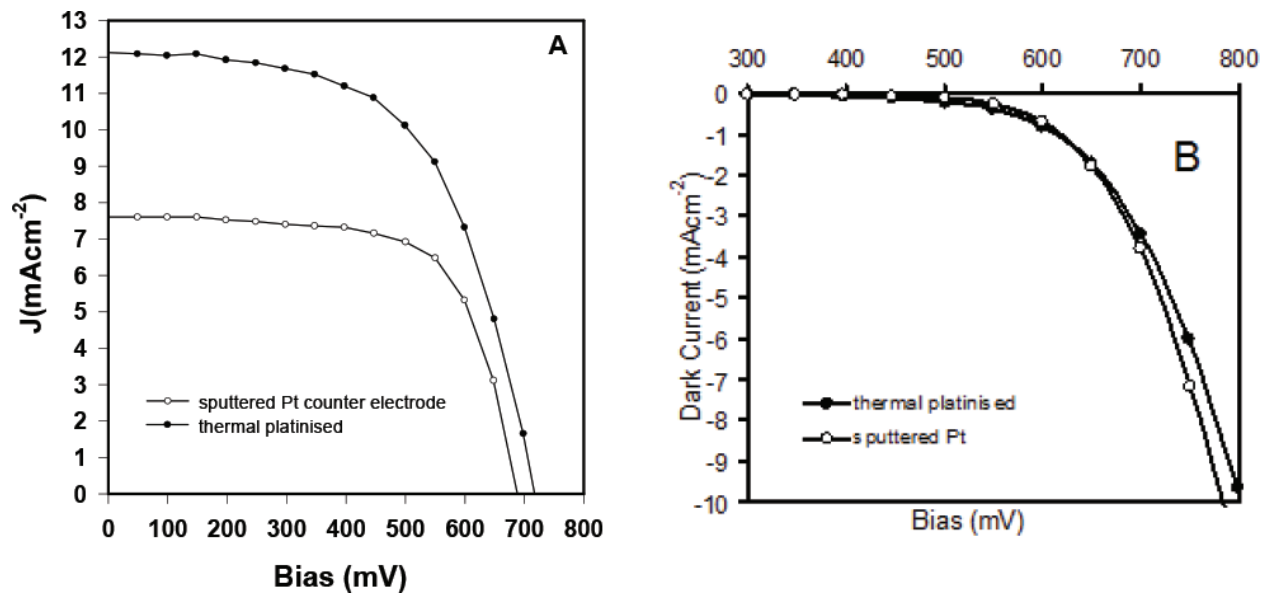


Figure 10. I-V curves of mesoporous titania derived from neutral hydrothermal route using different platinization methods for counter electrodes: (A) light current and (B) the corresponding dark current curves [1].

counter electrodes. It is observed that the thermally platinized counter electrode gave better DSSC performance with increased open-circuit voltage (V_{oc}) and short-circuit current (I_{sc}). The increased variables enhanced the cell efficiency to about 5%. This improvement can be attributed to the high surface area of platinum in thermally platinized counter electrode that will act as an efficient catalyst for iodine reduction [8]. The redox electrolyte shuttles the electron from the site of regeneration on the sensitized titania working electrode to the counter electrode to complete the electron cycle. During this process, the iodine must be reduced back to iodide at minimum energy loss on the counter electrode. However, the fill factor of this cell is much lower than that assembled with a sputtered Pt counter electrode. This may be caused by the loss of some scattered light, which may enhance the electron generation throughout the titania film. The possible recombination rate for this thermally platinized cell is slightly lower than that of the sputtered Pt counter electrode. Thus, it is expected to compromise the losses. In addition, this type of counter electrode produced a transparent DSSC. Illumination can be performed in both sides of the sandwiched cells that cannot be done by using sputtered Pt counter electrode.

Comparing the performance of acid treated-acid route photoanode with neutral route, a higher efficiency was achieved for the latter photoanode [1]. High open-circuit voltage and short-circuit current are responsible for this performance, which may be caused by the presence of the full anatase domain characteristic of the powder precursor as previously demonstrated (Section 1).

Table 4 shows the solar cell parameters of various titania photoanodes and natural dyes as sensitizers. Results on natural dyes as the sensitizers are not as high as the cells using ruthenium complex. Dried fruit of *joho*, bark of *tingi*, and *tegeran* were commonly used as dyes for traditional *Batik* clothes in Indonesia. The cells with *joho* and *tegeran* dyes have shown appreciable generated photovoltage and photocurrent compared to *tingi*. Both *joho* and *tegeran* dyes

Sample	V _{oc} (mV)	J _{sc} (mA/cm ²)	Fill factor (FF, %)	η (%)
Neutral route meso-Ti-sputtered Pt counter electrode*	688	7.60	68.14	3.56
Neutral route meso-Ti-thermal platinized counter electrode*	717	12.12	58.11	5.05
Acid treated-acid route meso-Ti-thermal platinized counter electrode*	666	11.24	62.40	4.67
Joho (<i>Terminalia bellirica(gaertn)roxb</i>)**	100	1.60	31.00	0.19
Tingi (<i>Ceriops tagal</i>)**	70	0.80	21.00	0.05
Tegeran (<i>Maclura cochinchensis</i>)**	100	1.60	38.00	0.24
Bixin extract (<i>Bixa orellana</i> L.) and nanotube TiO ₂ 60 min stirring prior hydrothermal***	310	3.10	44.08	1.48
Bixin extract (<i>Bixa orellana</i> L.) and commercial titania electrode***	749	8.50	28.29	0.42
<i>Sargassum mclurei</i> Setchell**	60	0.30	25.00	0.09
<i>Hypnea esperi</i> Bory**	55	1.30	31.00	0.44

*Testing done at photovoltaic testing facility in Physics Department, University of Queensland, Brisbane, Australia, across a 0.025 cm² active area DSSC under illumination of 100 mW/cm² power source equal to AM1.5 Direct Sun, sensitizer ruthenium N3 dye.

**Active area TiO = P25 0.25 cm²; P_{input} = 25.6 mW/cm², Au counter electrode, testing done in Physics Department, Universitas Gadjah Mada, Yogyakarta, Indonesia.

***Testing done in Universitas Negeri Sebelas Maret, Surakarta, Indonesia.

Table 4. Solar cell parameters of various titania photoanodes and natural dyes as sensitizers.

have absorption spectra indicating reasonable composition of red-shift absorption maxima and blueshift absorption edges, while *tingi* dye has slightly low red-shift and blueshift contribution (data not shown). Upon adsorption on a TiO₂ layer, the absorption spectra of the three *Batik* dyes are all broadened forward to red side compared with their respective spectra in ethanol solution. These indicate sensitizing effect of natural *Batik* dyes on TiO₂ films [34, 35]. The small red-shift of the absorption maxima suggests the absence of the formation of *J*-like aggregates which was predicted to lower the photocurrent efficiency in DSSC [36]. Thus, the natural *Batik* dyes used are predicted mostly in the monomer form. However, the absorption edges were shifted with the large blueshift of 85–165 nm, which may be induced by the formation of *H*-aggregates. In contrast with *J*-aggregates, the formation of *H*-aggregates supports efficient ability of the dyes for sensitization [36]. Low sensitization effect may occur owing to self-quenching of the dyes in the *J*-like aggregate form.

Results on Bixin extract of achiote (*Bixa orellana* L.) seed as sensitizer has shown relatively higher efficiency sensitizer than the *Batik* dyes. It also confirms that nanotube titania performs better than commercial titania which has nanoparticle structure. Whereas algae’s dyes (the latter two) have comparable performance as *Batik* dyes and bixin of around 0.1-0.5%. Large difference in photocurrent density of the two cells rather than in photovoltage suggests that the solar cell performance of the cells is influenced by the efficiency of the electron injection from the sensitizers into TiO₂ [1]. High photocurrent resulted from efficient electron injection of the pigments into the conduction band of TiO₂ owing to the effective attachment of the pigment molecules on the TiO₂ surface.

4. Titania as active component for multifunctional coatings

Crystalline TiO_2 (titanium dioxide), anatase, is widely known as material having excellent photocatalytic properties. Anatase coatings have also been prepared by a number of deposition techniques, such as sputtering, spray pyrolysis [37], and sol–gel processing [38]. The film formations are aimed at finding more flexible application in electronic devices, optical coatings, instrument hard coatings, and decorative parts. They are also generating different functionalities by engineering the surface, saving the energy consumption in production, and minimalizing the use of toxic materials since the quantity used is limited only to the surface and/or thin film layer. Thus, the film formation is an environmentally benign material technology and fits well to the current global trend of sustainable chemistry concept. However, sol–gel methods usually require a heating process at relatively high temperatures above 400°C to obtain sufficient crystallinity [39]. Thus, anatase coatings on organic substrates and incorporation of organic molecules into the coatings were not directly achieved using these techniques. TiO_2 layers on organic substrates are mostly amorphous, while the photoactivity of amorphous phase of TiO_2 has been less studied and explored. In this section, self-cleaning titania coating on textile will be discussed, as well as antibacterial functional. Recent results on coating of titania on wood as antifouling agent will also be explored.

Self-cleaning and antibacterial coatings on textile. This study aims at preparing amorphous and crystalline TiO_2 coating on cotton fabrics and examining the discoloration of organic materials modeled by turmeric extract stain on the cotton textile coated with those TiO_2 . Turmeric extract obtained from rhizomes of *Curcuma longa* is one of the main pigments produced in Brazil [10]. Besides the yellow pigment for food, this plant is widely used as a seasoning for Asian food including Indonesian food. Mature rhizomes are ground to give an aromatic yellow powder, employed as the coloring ingredient in curry powder. With the growing demand for natural colors, the use of turmeric is likely to increase. Therefore, turmeric extract stain is used as the model stain for self-cleaning action. It is also reported that amorphous TiO_2 coating on cotton fabrics has self-cleaning action similar to the crystalline TiO_2 coating but lower activity. The use of TiO_2 -loaded flexible substrates will possibly allow their application for the photodegradation of micelles, oils, solvents, sooth, and aromatic and aliphatic hydrocarbons under daylight.

The white cotton textiles were purchased from local market after examining the burning characteristic of cotton fibers. Pure cotton fibers gave only black gray ash after burning. Turmeric powders were also obtained from local market. All the reagents are of analytical grade and used without further purification. Titanium (IV) tetraisopropoxide (TTIP 97%, Aldrich) and TiO_2 powder of P25 (Degussa) were used as titanium sources. TiO_2 P25 was a gift from Degussa Germany. The pre-cleaned cotton fabrics were dipped into the Ti suspension and withdrawn vertically at the rate of 20 cm/min. The coating was repeated one, five, and fifteen times before dried naturally and cured at 100°C for 15 min. The cured coated cotton fabrics were then rinsed with distilled water in ultrasonic washer to wash out the unbonded TiO_2 for 5 min and dried at room temperature [40]. **Figure 11** displays the XRD patterns of amorphous and crystalline TiO_2 -coated cotton fabrics.

From **Figure 11** (left), it is evident that coating by employing hydrolyzed TTIP sols results in no observable crystalline TiO_2 diffraction peaks. The observed peaks were corresponding to the cellulose fibers of the cotton fabrics [41]. XRD pattern of xerogels obtained from drying the sol precursor used for coating displays very broad peaks around 2θ of $\sim 25^\circ$, suggesting that TiO_2 layers on the surface of cotton fabrics predominantly consisted of amorphous titania. After curing, the diffraction peaks of the coated cotton fabrics have decreased. It is presumably due to the sintering of both cellulose fibers and TiO_2 layers. The XRD patterns in **Figure 11** (right) shows that TiO_2 P25 coating resulted in crystalline peaks of anatase (A) TiO_2 at diffraction angle $\sim 25^\circ$ and rutile (R) TiO_2 at $\sim 27^\circ$. This is in accordance with the fact known that TiO_2 P25 powder consists of 80% anatase and 20% rutile crystalline phases [42]. Similar to **Figure 11** (left), the bulk of the XRD peaks originated from cotton, as cotton is the underlying substrate. As the thickness of the coating layers increased, which resulted from multiple coatings, both anatase and rutile peaks are getting more intense. These results are comparable to the work of Qi et al. [41], who has observed that anatase peaks are intensifying due to increased crystalline nature of the corresponding sol precursors. It is also observed that the thicker the TiO_2 coating, the weaker the cotton. This may be attributed to titania coatings on cotton which shield the X-ray beam, therefore weakening the intensities of the peaks of cotton coated with titania [41, 43]. The structure and morphology of TiO_2 layers on cotton fabrics were investigated by using scanning electron microscopy (SEM) as depicted in Figure 4.

SEM images (**Figure 12**) of the coatings on cotton fabrics show that the surface structures of the two titania-coated cotton fabrics look similar. The surface structure of these titania-coated cotton fibers shows that a thick uniform layer has been formed. The low-resolution image

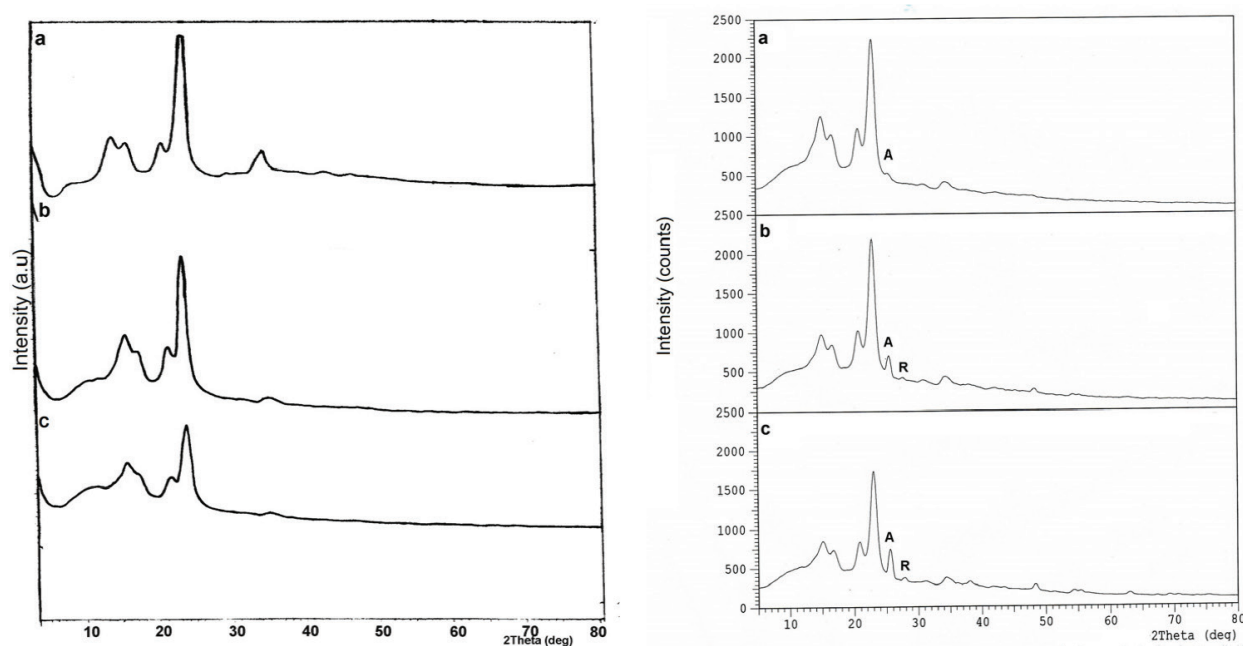


Figure 11. The XRD patterns of samples (left): (a) pristine cotton fabrics, (b) cotton fabrics coated with amorphous TiO_2 from 0.2 M Ti precursor, and (c) cotton fabrics coated with amorphous TiO_2 from 0.2 M Ti sol precursor after curing at 120°C for 1 h. P25-coated (right): (a) 1 \times , (b) 5 \times , and (c) 15 \times coatings with curing.

of the pristine cotton fibers (**Figure 12a**) has shown no such uniform layers on the surface. **Figure 12b and c** has also confirmed TiO_2 layers covering the surface of cotton fibers. This type of coating is similar as obtained by Qi et al. [41] for TiO_2 and for chitosan coating on textiles [44, 45]. However, the formation of interconnected layers over the fibers as observed for thicker coating of chitosan on textiles [45] was not observed for this TiO_2 coating suggesting bigger particle size of the coating materials. It is supposed that smaller particles have more tendencies to form polymeric-like network due to smaller solvation spheres.

The self-cleaning effect of TiO_2 -coated white cotton fabrics was evaluated by the decomposition of turmeric extract stains in ethanolic solution under UV light irradiation. **Figure 13** displays the self-cleaning performance of amorphous (a)- and crystalline (b)-coated cotton fabrics under (light) and without (dark) UV illumination.

It is clear that the TiO_2 P25-coated cotton fabrics which have crystalline nature of TiO_2 layers demonstrate higher photoactivity than the amorphous. The mechanism of decomposition of colorant molecules on titania under UV irradiation is widely known suggesting the generation

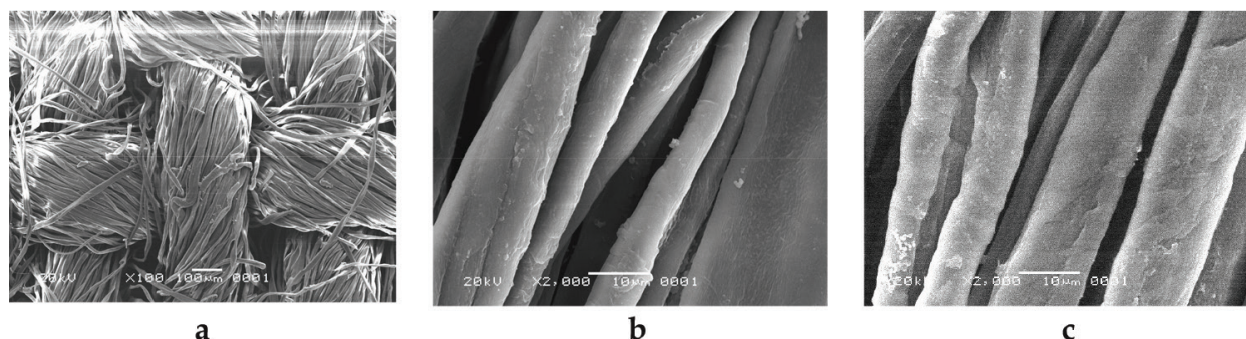


Figure 12. The SEM images of (a) pristine cotton fabrics, (b) cotton fabrics coated by amorphous TiO_2 from 0.1 M Ti precursor, and (c) cotton fabrics coated by amorphous TiO_2 from 0.2 M Ti precursor.

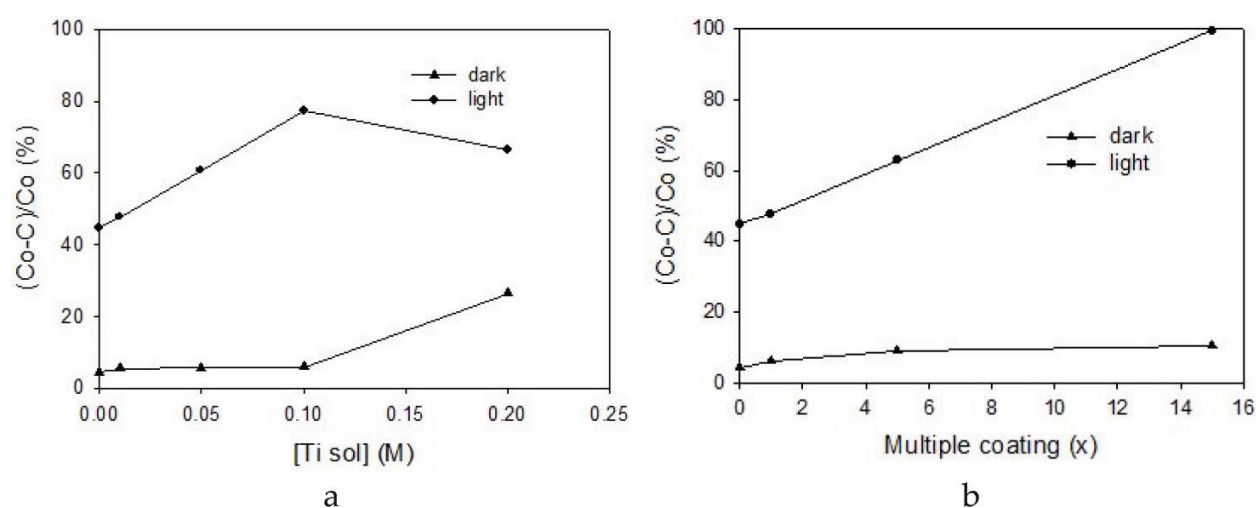


Figure 13. Self-cleaning action at alternated Ti loading of (a) amorphous TiO_2 -coated cotton fabrics and (b) crystalline TiO_2 -coated cotton fabrics.

of highly oxidative radicals on the TiO_2 surface when light below 400 nm is applied on the TiO_2 photocatalyst surface [42, 46]. **Figure 14** shows the color difference of the self-cleaning action on the coated and uncoated cotton.

The 15 times coating of TiO_2 P25-coated cotton fabrics have the highest self-cleaning action which is considered to be attributed to the highest anatase crystallinity as demonstrated by its sharpest anatase peaks with greatest intensities from the XRD studies in **Figure 12**. From these self-cleaning testing, it is worth noting that the amorphous coating has demonstrated significant photocatalytic activity toward turmeric stain discoloration reaching almost 80% discoloration. The mechanism behind this is still unclear and needed further investigation.

Antibacterial coatings on textile. To enhance crystallization of amorphous titania coating on textiles, exposure of the coated cotton to water vapor for certain times was performed. Introduction of silica on titania coating was also done to enhance the mechanical strength of the coated titania on fabrics [47]. This section will discuss antibacterial properties of the coated cotton with TiO_2 - SiO_2 against bacteria *E. coli* by counting the bacteria before and after testing using colony counter technique. The XRD patterns of the vapor treated coated cotton are shown in **Figure 15a**, and the antibacterial test results are in **Figure 15b**.

Based on the XRD patterns (**Figure 15a**), diffraction peaks of crystalline cellulose as the major component of the cotton fabrics are prominent, with the highest at $2\theta \sim 23$ of d_{002} [4]. It can be seen that the higher the amount of Ti, the peak intensity tends to decrease. A very small hump was observed at sample with Ti:Si 3:1, indicating the presence of anatase titania. It also appears that the peak intensity decreases as increasing the Ti content showing the thick coating of Si-Ti on the cotton fiber. The antibacterial activities of the coated cottons are comparable to the commercial antibacterial cloth, which is Ag-coated. It is worth to note that the coated cotton without exposure to water vapor has almost similar inhibition compared to the ones that have been exposed. This supports the photoactivity of amorphous titania and the fact that the antibacterial coating is active even without UV irradiation.

Antifouling coatings on wood. Fouling has been a big problem for infrastructure in the sea. Algae, mollusks including zebra mussels and barnacles, wood boring worms, and also critters like to make the hull their home and can seriously affect the performance of a boat. The current antifouling agents are mostly based on organo-tin, which is highly toxic; therefore

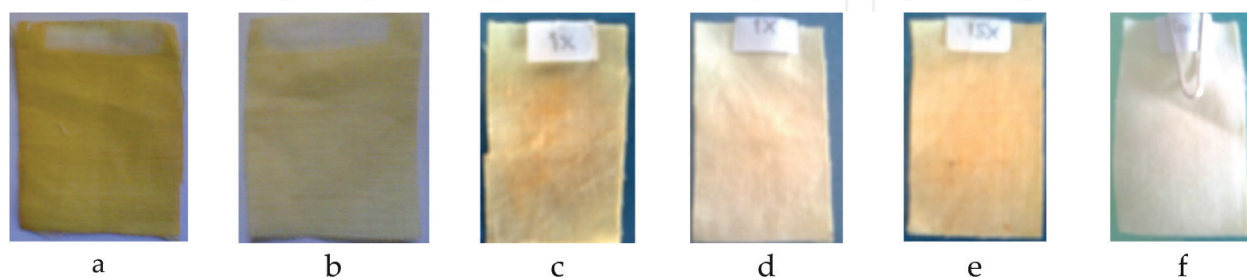


Figure 14. Discoloration of coated cotton before UV illumination: (a) amorphous titania, (c) 1 time coating, and (e) 15 times coating of P25 titania; and after UV illumination: (b) amorphous titania, (d) 1 time coating, and (f) 15 times coating of P25 titania.

coating of nanorod-TiO₂ and SiO₂ on wood is proposed. The antifouling mechanism is expected from combined effect of surface hydrophobicity and photocatalysis. Nanorod morphology is expected to build the surface roughness as well as photoactive agent [48]. The silica will provide sturdy coating formulation in the acrylic-based paints. **Figure 16** shows our prompt results on antifouling test of the coated woods in the sea water. Clean surface of wood was achieved for the coated wood, both by TiO₂-nanorod and TiO₂-nanorod-SiO₂. More quantitative data and elaboration on mechanism are on progress [49].

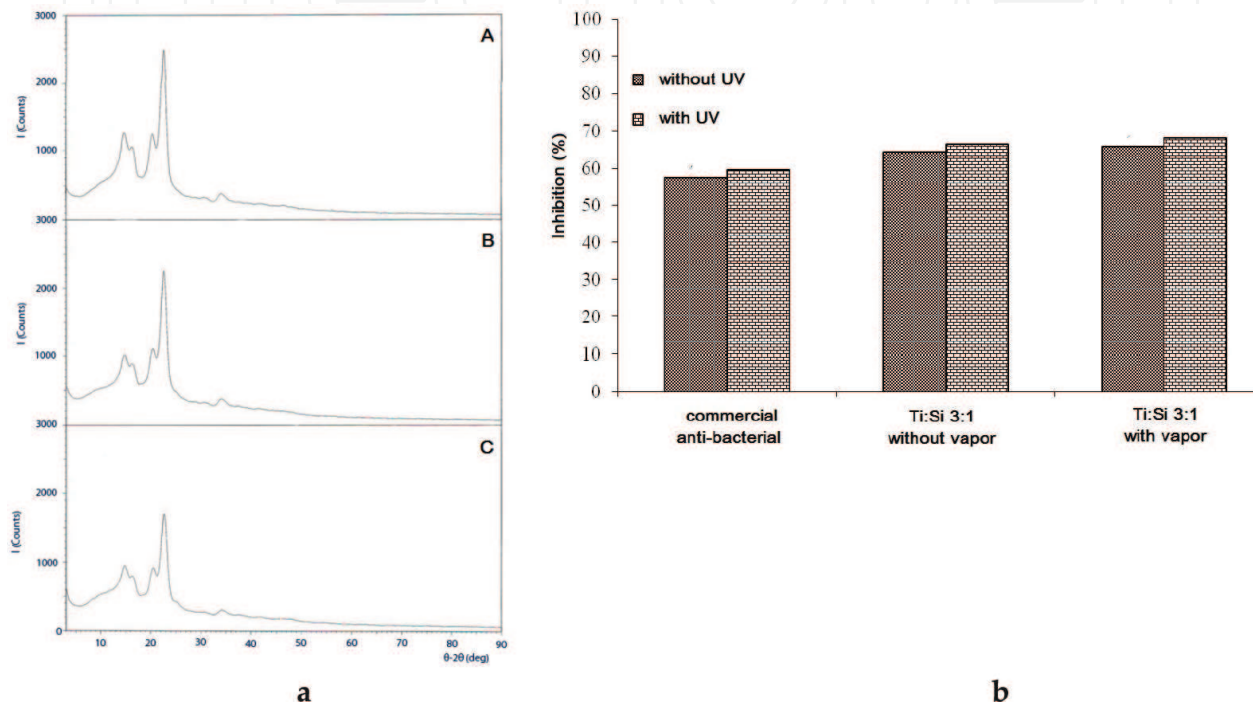


Figure 15. (a) XRD patterns of cotton fabrics coated by Ti:Si (A) 0:1, (B) 1:0, and (C) 2:1; (b) antibacterial test of commercial antibacterial cloth and cotton fabrics coated with silica-titania with Ti:Si 3:1 which are exposed and not exposed to water vapor.

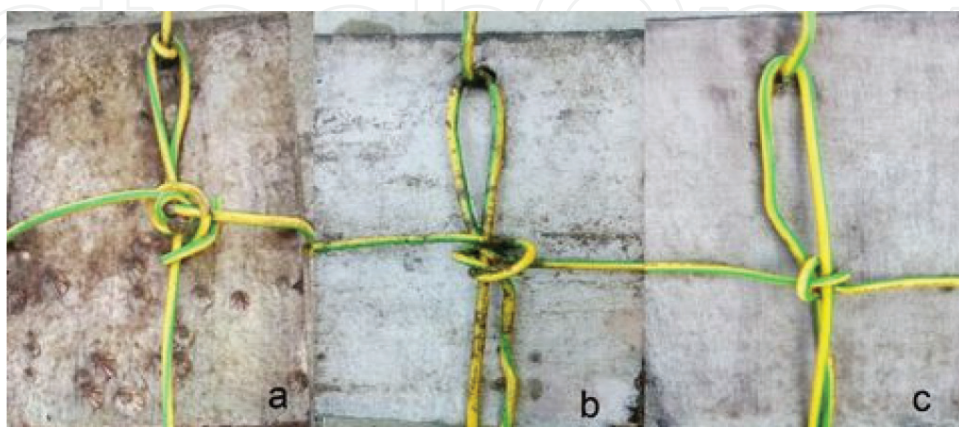


Figure 16. Antifouling test in the sea water: (a) uncoated wood, (b) TiO₂-nanorod-coated wood, and (c) TiO₂-nanorod/SiO₂-coated wood.

5. Concluding remarks

It has been shown that hydrothermal-seeded technique offered excellent method to obtain mesostructured titanium dioxide with large porosity and full anatase domain ideal as photoanodes on photoelectrochemical solar cell. Designing the morphology of titanium dioxide into 1D titania such as nanotube has also resulted in improved solar photoconversion due to enhanced surface area. Alteration of morphology into nanotube also has induced photoactivity to be visible-responsive photocatalyst. Mechanical mixing prior hydrothermal synthesis provided the way to shorten the preparation of nanotube titania to the shortest time as long as 5 h.

By applying dip coating and sol-gel precursor preparation of titanium, amorphous and nanocrystalline anatase/rutile coatings have been successfully deposited on cotton fabrics at near room temperature. Both coated fabrics have shown significant self-cleaning action toward decoloration of turmeric extract stains reaching almost full decoloration under UV illumination for the crystalline TiO_2 -coated cotton fabrics. The higher the crystallinity of anatase TiO_2 , the higher the degree of the photodecoloration. Our study also revealed that amorphous TiO_2 coating has demonstrated about 80% photodecoloration and about 60% antibacterial inhibition against *E. coli*. Excellent coatings of TiO_2 nanorod on wood have provided antifouling activity by testing in sea water. More studies on characterization and mechanism are being underway.

Acknowledgements

The authors acknowledge the Ministry of Research, Technology, and Higher Education of the Republic of Indonesia (PBK 2017-2018, Stranas 2007, RUT 2005), International Foundation for Science Sweden (the second grant), and Universitas Gadjah Mada for financial supports.

Author details

Indriana Kartini^{1*}, Inna Yusnita Khairani¹, Chotimah², Kuwat Triyana² and Sri Wahyuni³

*Address all correspondence to: indriana@ugm.ac.id

¹ Department of Chemistry, Faculty of Mathematics and Natural Sciences, Universitas Gadjah Mada, Yogyakarta, Indonesia

² Physics Department, Faculty of Mathematics and Natural Sciences, Universitas Gadjah Mada, Yogyakarta, Indonesia

³ Department of Chemistry, Faculty of Mathematics and Natural Sciences, Universitas Negeri Semarang, Semarang, Indonesia

References

- [1] Kartini I, Menzies D, Blake D, da Costa JCD, Meredith P, Riches JD, Lu GQ. Hydrothermal seeded synthesis of mesoporous titania for application in dye-sensitised solar cells (DSSCs). *Journal of Materials Chemistry*. 2004;**14**:2917-2921
- [2] Kartini I, Meredith P, Da Costa JCD, Lu GQ. A novel route to the synthesis of mesoporous titania with full anatase nanocrystalline domains. *Journal of Sol-Gel Science and Technology*. 2004;**31**:185-189
- [3] Meredith P, Powell BJ, Riesz J, Vogel R, Blake D, Kartini I, Will G, Subianto S. Broadband Photon-Harvesting Biomolecules for Photovoltaics. In *Artificial Photosynthesis*. Weinheim: Wiley-VCH; 2005
- [4] Kartini I, Ilmi I, Kunarti ES, Kamariah. Wash fastness improvement of malachite green-dyed cotton fabrics coated with nanosol composites of silica-Titania. *Bulletin of Materials Science*. 2014;**37**(6):1419-1426
- [5] Zhang Z, Han Y, Xiao FS, Qiu S, Zhu LWR, Yu Y, Zhang Z, Zou B, Wang Y, Sun H, Zhao D, Wei Y. Mesoporous aluminosilicates with ordered hexagonal structure, strong acidity, and extraordinary hydrothermal stability at high temperatures. *Journal of the American Chemical Society*. 2001;**123**(21):5014-5021
- [6] Liu Y, Zhang W, Pinnavaia TJ. Steam-stable MSU-S aluminosilicate mesostructures assembled from zeolite ZSM-5 and zeolite beta seeds. *Angewandte Chemie International Edition*. 2001;**40**(7):1255-1258
- [7] Pinnavaia TJ, Pauly TR, Kim S-S. Process for the preparation of hybrid mesoporous molecular sieve silicas from amine surfactants. *Studies in Surface Science and Catalysis*. 2001;**135**(Zeolites and Mesoporous Materials at the Dawn of the 21st Century):1337-1344
- [8] Liu J, Zhang X, Han Y, Xiao F-S. Direct observation of nanorange ordered microporosity within mesoporous molecular sieves. *Chemistry of Materials*. 2002;**14**(6):2536-2540
- [9] Wang YQ, Ying JY. Sol-gel synthesis and hydrothermal processing of anatase and rutile titania nanocrystals. *Chemistry of Materials*. 1999;**11**:3113-3120
- [10] Yanagisawa K, Ovenstone J. Crystallization of anatase from amorphous titania using the hydrothermal technique: Effect of starting material and temperature. *The Journal of Physical Chemistry. B*. 1999;**103**:7781-7787
- [11] Yang PD, Zhao DY, Margolese DI, Chmelka BF, Stucky GD. Block copolymer templating syntheses of mesoporous metal oxides with large ordering lengths and semicrystalline framework. *Chemistry of Materials*. 1999;**11**(10):2813-2826
- [12] Yoldas BE. Hydrolysis of titanium alkoxide and effects of hydrolytic polycondensation parameters. *Journal of Materials Science*. 1986;**21**:1087-1092

- [13] Bradley DC, Mehrotra RC, Gaur DP. Metal Alkoxides. London: Academic Press Inc.; 1978
- [14] Brinker CJ, Scherer GW. Sol-Gel Science: The Physics and Chemistry of Sol-Gel Processing. San Diego: Academic Press Ltd.; 1990
- [15] Bosc F, Ayral A, Albouy P, Guizard C. A simple route for low-temperature synthesis of mesoporous and nanocrystalline anatase thin films. *Chemistry of Materials*. 2003;**15**:2463
- [16] Yang PD, Zhao DY, Margolese DI, Chmelka BF, Stucky GD. Generalized syntheses of large-pore mesoporous metal oxides with semicrystalline frameworks. *Nature*. 1998;**396**(6707):152-155
- [17] Alberius PCA, Frindell KL, Hayward RC, Kramer EJ, Stucky GD, Chmelka BF. General predictive syntheses of cubic, hexagonal, and lamellar silica and titania mesostructured thin films. *Chemistry of Materials*. 2002;**14**(8):3284-3294
- [18] Zhao D, Huo Q, Feng J, Chmelka BF, Stucky GD. Nonionic triblock and star diblock copolymer and oligomeric surfactant syntheses of highly ordered, hydrothermally stable, mesoporous silica structures. *Journal of the American Chemical Society*. 1998;**120**(24):6024-6036
- [19] Kleitz F, Choi SH, Ryoo R. Cubic Ia3d large mesoporous silica: Synthesis and replication to platinum nanowires, carbon nanorods and carbon nanotubes. *Chemical Communications*. 2003;**17**:2136-2137
- [20] Wanka G, Hoffmann H, Ulbricht W. Phase diagrams and aggregation behavior of poly (oxyethylene)-poly (oxypropylene)-poly (oxyethylene) triblock copolymers in aqueous solutions. *Macromolecules*. 1994;**27**:4145-4159
- [21] Su Y-l, Wang J, Liu H-Z. FTIR spectroscopic investigation of effects of temperature and concentration on PEO-PPO-PEO block copolymer properties in aqueous solutions. *Macromolecules*. 2002;**35**:6426-6461
- [22] Kasuga T, Hiramatsu M, Hoson A, Sekino T, Niihara K. Formation of titanium oxide nanotube. *Langmuir*. 1998;**14**(12):3160-3163
- [23] Bavykin DV, Walsh FC. Titanate and Titania Nanotubes. Cambridge: RSC; 2010
- [24] Sikhwivhilu LM, Sinha Ray S, Coville NJ. Influence of bases on hydrothermal synthesis of titanate nanostructures. *Applied Physics A: Materials Science and Processing*. 2009;**94**(4):963-973
- [25] Liu P, Zhang H, Liu H, Wang Y, Yao X, Zhu G, Zhang S, Zhao H. A facile vapor-phase hydrothermal method for direct growth of titanate nanotubes on a titanium substrate via a distinctive nanosheet roll-up mechanism. *Journal of the American Chemical Society*. 2011;**133**(47):19032-19035
- [26] Bach U, Lupo D, Comte P, Moser JE, Weissortel F, Salbeck J, Spreitzer H, Gratzel M. Solid-state dye-sensitized mesoporous TiO₂ solar cells with high photon-to-electron conversion efficiencies. *Nature*. 1998;**395**:583-585

- [27] Stone JL. Photovoltaics: Unlimited electrical energy from the sun. *Physics Today*. 1993;**46**(9):22
- [28] Nazeeruddin MK, Kay A, Rodicio I, Humphry-Baker R, Muller E, Liska P, Vlachopoulos N, Gratzel M. Conversion of light to electricity by cis-X₂Bis(2,2'-bipyridil-4,4'-dicarboxylate)ruthenium(II) charge-transfer sensitizers (X=Cl-, Br-, I-, CN-, and SCN-) on nanocrystalline TiO₂ electrodes. *Journal of the American Chemical Society*. 1993;**115**:6382-6390
- [29] Gratzel M. Perspectives for dye-sensitized nanocrystalline solar cells. *Progress in Photovoltaics: Research and Applications*. 2000;**8**:171-185
- [30] Morgado E, de Abreu MAS, Moure GT, Marinkovic BA, Jardim PM, Araujo AS. Effects of thermal treatment of nanostructured tititanates on their crystallographic and textural properties. *Materials Research Bulletin*. 2007;**42**(9):1748-1760
- [31] Turki A, Kochkar H, Guillard C, Berhault G, Ghorbel A. Effect of Na content and thermal treatment of titanate nanotubes on the photocatalytic degradation of formic acid. *Applied Catalysis B: Environmental*. 2013;**138-139**:401-415
- [32] Kartini I, Khairani IY, Mustofa S, Santosa SJ, Wang L. The effect of alkaline ratios of NaOH to NH₃ on the formation of nanostructured titania. *Materials Science Forum*. 2017;**886**:42-47
- [33] Kartini I, Jannah INA, Amalia FR, Mustofa S, Kunarti ES, Swasono RT. Short-time synthesis of titania nanotubes: The effect of pre-mixing prior hydrothermal. *Indonesian Journal of Chemistry*. 2018. Submitted
- [34] Nazeeruddin MK, Pechy P, Renouard T, Zakeeruddin SM, Humphry-Baker R, Comte P, Liska P, Cevey L, Costa E, Shklover V, Spiccia L, Deacon GB, Bignozzi CA, Gratzel M. Engineering of efficient panchromatic sensitizers for nanocrystalline TiO₂-based solar cells. *Journal of the American Chemical Society*. 2001;**123**:1613-1624
- [35] Yao Q-H, Meng F-S, Li F-Y, Tian H, Huang C-H. Photoelectric conversion properties of four novel carboxylated hemicyanine dyes on TiO₂ electrode. *Journal of Materials Chemistry*. 2003;**13**:1048-1053
- [36] Dai Q, Rabani J. Photosensitization of nanocrystalline TiO₂ films by anthocyanin dyes. *Journal of Photochemistry and Photobiology A: Chemistry*. 2002;**148**:17-48
- [37] Sayama K, Tsukagoshi S, Mori T, Hara K, Ohga Y, Shinpou A, Abe Y, Suga S, Arakawa H. Efficient sensitization of nanocrystalline TiO₂ films with cyanine and merocyanine organic dyes. *Solar Energy Materials and Solar Cells*. 2003;**80**:47-71
- [38] Yanagi H, Ohoka Y, Hishiki T, Ajito K, Fujishima A. Characterization of dye-doped TiO₂ films prepared by spray-pyrolysis. *Applied Surface Science*. 1997;**113-114**:426-431
- [39] Yoko T, Yuasa A, Kamiya K, Sakka S. Sol-Gel-Derived TiO₂ Film Semiconductor Electrode for Photocleavage of Water: Preparation and Effects of Postheating Treatment on the Photoelectrochemical Behavior. *Journal of the Electrochemical Society*. 1991;**138**: 2279-2285

- [40] Manzan ACM, Toniolo FS, Bredow E, Povh NP. Extraction of Essential Oil and Pigments from *Curcuma longa* [L.] by Steam Distillation and Extraction with Volatile Solvents. *Journal of Agricultural and Food Chemistry*. 2003;**51**(23):6802-6807
- [41] Vainio U. Report Series in Physics: HU-P-D145. Finlandia: Helsinki University Printing House; 2007
- [42] Qi K, Daoud WA, Xin JH, Mak CL, Tanga W, Cheung WP. Self-cleaning cotton. *Journal of Materials Chemistry*. 2006;**16**:4567-4574
- [43] Hoffmann MR, Martin SM, Choi W, Bahnemann DW. Environmental Applications of Semiconductor Photocatalysis. *Chemical Reviews*. 1995;**95**:69-96
- [44] Bozzi A, Yuranova T, Kiwi J. Self-cleaning of wool-polyamide and polyester textiles by TiO₂-rutile modification under daylight irradiation at ambient temperature. *Journal of Photochemistry and Photobiology A: Chemistry*. 2005;**172**:27-34
- [45] Ye W, Leung MF, Xin J, Kwong TL, Lee DKL, Li P. Novel core-shell particles with poly(*n*-butyl acrylate) cores and chitosan shells as an antibacterial coating for textiles. *Polymer*. 2005;**46**:10538-10543
- [46] Kartini I, Andriani LK. Functionalization of textiles by chitosan coating. In: *Proceeding of 14th Regional Symposium on Chemical Engineering 2007*; AM33, 4-5th December 2007; Yogyakarta-Indonesia: Chemical Engineering Department, Gadjah Mada University. 2007. ISBN 978-979-16978-0-4
- [47] Linsebigler AL, Lu C, Yates JT. Photocatalysis on TiO₂ Surfaces: Principles, Mechanisms, and Selected Results. *Chemical Reviews*. 1999;**95**:735-758
- [48] Hayakawa S, Liu JF, dan Tsuru K. Wet deposition of titania-apatite in cotton fibrils. *Journal of Sol-Gel Science and Technology*. 2006;**40**:253-258
- [49] Wahyuni S, Kunarti ES, Swasono RT, Kartini I. Study on the properties and photoactivity of TiO₂(nanorod)-SiO₂ synthesized by sonication technique. *Oriental Journal of Chemistry*. 2017;**33**:249-257